https://doi.org/10.5194/egusphere-2026-2198
Preprint. Discussion started: 20 May 2026

East Asian Anthropogenic Aerosols Strongly Influence Past and Present Southern African Hydroclimate and Ecosystem Changes

Bosi Sheng[1,2,*], Massimo A. Bollasina[2], Alexandre S. Gagnon[3], Laura J. Wilcox[4], Thomas P. S. Reynolds[1], Christopher T. S. Beckett[1], Haolin Wang[2], Qingxiang Li[5], Pierre Nabat[6], Robert J. Allen[7], Bjørn H. Samset[8], Joonas Merikanto[9], Geeta G. Persad[10], Toshihiko Takemura[11], Kostas Tsigaridis[12,13], Sharar Ahmadi[4], Maxwell T. Elling[14,15], Knut von Salzen[16,17], Daniel M. Westervelt[18], Naga Oshima[19], Tsuyoshi Koshiro[19]

[1] Institute for Infrastructure and Environment, School of Engineering, University of Edinburgh, UK
[2] School of GeoSciences, University of Edinburgh, UK
[3] School of Biological and Environmental Sciences, Liverpool John Moores University, UK
[4] National Centre for Atmospheric Science, Department of Meteorology, University of Reading, UK
[5] School of Atmospheric Sciences, Sun Yat-Sen University, and Key Laboratory of Tropical Atmosphere-Ocean System, Ministry of Education, China
[6] Météo-France, CNRS, Université de Toulouse, CNRM, Toulouse, France
[7] Department of Earth and Planetary Sciences, University of California Riverside, Riverside, CA, USA
[8] CICERO Center for International Climate Research, Oslo, Norway
[9] Finnish Meteorological Institute, Climate Research, Helsinki, Finland
[10] Department of Geological Sciences, The University of Texas at Austin, Austin, TX, USA
[11] Research Institute for Applied Mechanics, Kyushu University, Fukuoka, Japan
[12] Center for Climate Systems Research, Columbia University, New York, NY, USA
[13] NASA Goddard Institute of Space Studies, New York, NY, USA
[14] Department of Atmospheric and Oceanic Sciences, University of Colorado Boulder, Boulder, CO, USA
[15] Cooperative Institute for Research in Environmental Sciences, University of Colorado Boulder, Boulder, CO, USA
[16] Canadian Centre for Climate Modelling and Analysis, Environment and Climate Change Canada, Victoria, BC, Canada
[17] Department of Atmospheric and Climate Science, University of Washington, Seattle, WA, USA
[18] Lamont-Doherty Earth Observatory, Columbia University, New York, NY, USA
[19] Meteorological Research Institute, Japan Meteorological Agency, Ibaraki, Japan

Correspondence: Bosi Sheng (bsheng@ed.ac.uk)

Abstract. Southern Africa (SA) is highly sensitive to rainfall changes, as water availability significantly influences agriculture, ecosystems, and the region's socio-economic stability. Observations reveal substantial multi-decadal changes

https://doi.org/10.5194/egusphere-2026-2198
Preprint. Discussion started: 20 May 2026

in December–February precipitation during the second half of the 20th century, characterized by enhanced rainfall over the southern part of SA (hereafter SSA), including Madagascar (MDG), and drying to the north. More recently, however, this long-term wetting tendency has reversed, with widespread drying observed across much of the region since the mid-2000s. Despite their global significance, their impact of anthropogenic aerosols on southern African precipitation has received limited attention, and the underlying mechanisms remain unclear. We show that East Asian (EAS) anthropogenic aerosols played a key role in driving enhanced precipitation over SSA and MDG between 1945 and 2005, alongside the influence of internal variability. Increased EAS sulfate emissions strengthened interhemispheric temperature and pressure gradients, inducing a southward shift of the Intertropical Convergence Zone and associated Hadley circulation, thereby enhancing moisture convergence over SSA and MDG. After the mid-2000s, rapid reductions in EAS aerosols reversed this circulation response and contributed to declining precipitation. Applying this physical framework to near-future scenarios from the Regional Aerosol Model Intercomparison Project further suggests that continued reductions in aerosols will lead to further hydroclimatic adjustments. The recent decline in precipitation (2006–2020) coincides with reduced gross primary productivity and leaf area index, as well as intensified fire-weather conditions. These findings highlight the sensitivity of southern African hydroclimate and ecosystems to remote anthropogenic aerosol emissions.

1 Introduction

Southern Africa (SA), including the adjacent southwest Indian Ocean and Madagascar (MDG), is frequently affected by both droughts and floods, with more than 95 % of agricultural production dependent on seasonal precipitation (Ashfaq et al., 2021; Kephe et al., 2021). Owing to its limited adaptive capacity and high exposure to climate variability, SA is widely regarded as one of the most climate-vulnerable regions on the African continent (Bedeke, 2023; Ansah et al., 2024). Improving our understanding of precipitation variability and its causes is essential for managing water resources, improving agricultural productivity, and ensuring ecosystem sustainability in the face of ongoing climate change (Niles et al., 2015; Bartzke et al., 2018).

During the peak austral summer monsoon (December–February, DJF) , rainfall over SA is primarily associated with tropical low-pressure systems and occasional tropical cyclones propagating westward from the tropics (Barimalala et al., 2020; Ibebuchi, 2023). Rainfall variability is further modulated by meridional shifts of the Intertropical Convergence Zone (ITCZ), which control the seasonal onset and retreat of precipitation (Quagraine et al., 2019; Randriatsara et al., 2022). Beyond the seasonal cycle, rainfall over SA is strongly influenced by internal climate variability. On interannual timescales, the El Niño–Southern Oscillation represents the dominant mode, while variability in Indian Ocean SST and Pacific decadal variability can further modulate regional rainfall (Palmer et al., 2023; Cai et al., 2025). On longer timescales, historical rainfall trends across SA exhibit pronounced spatial heterogeneity (Kusangaya et al., 2014; Marumbwa et al., 2019; Thoithi et al., 2021). Several studies based on long-term observations during the 20th century (e.g., 1921–2015; 1960–2010) indicate regionally varying rainfall changes, with localized drying in the central and north-eastern regions and increases in parts of

https://doi.org/10.5194/egusphere-2026-2198
Preprint. Discussion started: 20 May 2026

the southern interior (MacKellar et al., 2014; Kruger and Nxumalo, 2017). In contrast, other analyses identify drying across parts of the region, particularly in the northern and southwestern areas, in more recent decades (Marumbwa et al., 2019; Lim Kam Sian et al., 2021). These contrasting results likely reflect a combination of regional-scale circulation variability, differences in analysis periods, and substantial observational uncertainties, especially in data-sparse regions. As a result, a coherent understanding of multidecadal rainfall trends and their underlying drivers over SA remains limited, particularly regarding the relative roles of external forcing, internal variability, and remote anthropogenic influences.

In addition to greenhouse gases (GHGs), anthropogenic activities emit large amounts of aerosols and their precursors, which have substantially increased since industrialization (Hoesly et al., 2018; McDuffie et al., 2020). Although their global effective radiative forcing is smaller than that of GHGs, aerosols exert an overall cooling influence that partially offsets greenhouse-gas-induced warming and remain the largest source of uncertainty in estimates of anthropogenic climate forcing (Andrews and Forster, 2020; Bellouin et al., 2020). Aerosols influence the climate system primarily by scattering and absorbing incoming solar radiation, thereby reducing the amount of shortwave radiation reaching the surface. This leads to surface cooling, thereby increasing lower-tropospheric stability and modifying the large-scale atmospheric circulation (Ming and Ramaswamy, 2009). Beyond this radiative effect and its associated rapid adjustments and feedbacks, aerosols can also affect precipitation through complex interactions with cloud microphysical processes, referred to as aerosol-cloud interactions (Rotstayn and Lohmann, 2002). By acting as cloud condensation nuclei, increased aerosol loading enhances cloud droplet number concentration, leading to higher cloud albedo (Twomey, 1977; Albrecht, 1989). Aerosols can also suppress precipitation efficiency, thereby prolonging cloud lifetime and modifying regional radiative and hydrological balances (Stier et al., 2024).

Due to their short atmospheric lifetime, anthropogenic aerosols exhibit pronounced spatial heterogeneity in both loading and associated climate forcing (Allen, 2015; Wilcox et al., 2019). This spatial heterogeneity generates strong regional temperature gradients, which in turn drive substantial changes in atmospheric circulation and enable remote influences, including over the surrounding oceans through ocean–atmosphere interactions (Fahrenbach et al., 2024; Gao et al., 2025). Indeed, the influence of remote forcing can outweigh that of local forcing (Shindell et al., 2012; Lewinschal et al., 2013). For example, 20th-century aerosol increases have been linked to a southward displacement of the ITCZ (Allen, 2015; Voigt et al., 2017; Shonk et al., 2020), severe droughts in the Sahel and Amazonia during the mid-1980s (Hirasawa et al., 2022; Zhang et al., 2022), and weakening of the South and East Asian monsoons (Bollasina et al., 2011; Undorf et al., 2018; Sun et al., 2026). Asian anthropogenic aerosols have also been shown to modify the Australian summer monsoon through large-scale circulation changes (Fahrenbach et al., 2024; Gao et al., 2025). Despite these advances, the link between long-term changes in aerosol emissions and multi-decadal rainfall variability remains widely debated (Li et al., 2016; Wang et al., 2022). Attribution is particularly challenging due to the combined effects of internal variability, model biases, and inter-model differences in simulated responses (Saha and Ghosh, 2019; Liu et al., 2024).

https://doi.org/10.5194/egusphere-2026-2198
Preprint. Discussion started: 20 May 2026

Changes in precipitation caused by aerosols could significantly impact regional ecosystems. Vegetation plays a key role in the climate system by regulating exchanges of energy, water, and trace gases between the land surface and the atmosphere (Agossou and Kang, 2020; Humphrey et al., 2021). Precipitation is a primary climatic control on vegetation distribution and ecosystem productivity, not only through total rainfall amounts but also via its temporal characteristics, including frequency, intensity, seasonal distribution, and interannual variability (Gampe et al., 2021; Feldman et al., 2024b). Given the strong dependence of southern African ecosystems on seasonal rainfall, identifying the drivers of hydroclimatic variability is essential for effective environmental management and long-term ecosystem sustainability (Georganos et al., 2018).

Since the second half of the 20th century, anthropogenic aerosol and precursor emissions over Asia, particularly SO_2 over China, have undergone pronounced changes, characterized by a rapid increase followed by a subsequent decline in the early 21st century. While emissions over China have decreased markedly since the mid-2000s and emissions over South Asia (SAS) have continued to increase, reductions over East Asia (EAS) are sufficiently large to dominate the overall Asian trend, resulting in a net decline in aerosol forcing over recent decades (Hoesly et al., 2018; McDuffie et al., 2020; Zheng et al., 2020). Recent studies suggest that these reductions have already influenced global temperature (Samset et al., 2025), implying potential remote impacts on regional hydroclimate, including in SA. Given the strong hydroclimatic sensitivity of SA to precipitation changes, this provides a natural framework to examine the influence of East Asian aerosol forcing on regional rainfall. Here, we combine observations and climate model simulations to investigate this linkage. Section 2 describes the data and methods, Section 3 presents the results, and Section 4 discusses the findings and summarizes the main conclusions.

2 Data and Methods

2.1 Observational data

Monthly gridded land precipitation data were used to investigate multidecadal rainfall variability over Southern Africa (SA). For the period 1945–2005, precipitation was derived from the 0.5° × 0.5° Climate Research Unit dataset (CRU TS v4; (Harris et al., 2020)), which provides a long-term gauge-based record suitable for historical analysis. For the more recent period (2006–2020), precipitation was obtained from the TAMSAT dataset (Tropical Applications of Meteorology using SATellite data and ground-based observations; (Maidment et al., 2017), a satellite-based product specifically developed for data-sparse regions such as Africa. This choice is motivated by the substantial decline in gauge coverage in conventional datasets (e.g., CRU and GPCC) after 2000 (Becker et al., 2013; Harris et al., 2020), whereas TAMSAT provides consistent, high-resolution rainfall estimates constrained by satellite observations. The analysis was conducted by contrasting the two periods (1945–2005 and 2006–2020), which are characterized by opposite rainfall trends over SA. These periods also correspond to contrasting trends in East Asian aerosol emissions, increasing during 1945–2005 and decreasing during 2006–2020 (Fig. S1; (Hoesly et al., 2018; McDuffie et al., 2020). Temporal changes in precipitation

https://doi.org/10.5194/egusphere-2026-2198
Preprint. Discussion started: 20 May 2026

were quantified using least-squares linear trends. The analysis focused on austral summer (December–February, DJF), the primary rainy season in the region (Fig. S2). To isolate low-frequency variability, precipitation time series were smoothed using a Lanczos low-pass filter with a 10-year cutoff, removing variability at periods shorter than 10 years. Statistical significance was assessed using a two-tailed Student's t-test at the 90% confidence level. Monthly mean sea level pressure and 850 hPa winds used to characterize the background climatological circulation and circulation responses were obtained from the ECMWF Reanalysis v5 dataset (ERA5; (Hersbach et al., 2020)).

To assess observational robustness, the results were compared with independent precipitation datasets, including the Global Precipitation Climatology Centre dataset (GPCC; (Rustemeier et al., 2025)), the Global Precipitation Climatology Project dataset (GPCP; (Adler et al., 2003)), the CPC Merged Analysis of Precipitation (CMAP; (Xie and Arkin, 1997)). Annual anthropogenic emissions of SO_2 and BC over China and India were obtained from the Community Emissions Data System (CEDS; (Hoesly et al., 2018; McDuffie et al., 2020)) for the period 1900–2023.

2.2 CMIP6 simulations

We examined the role of anthropogenic forcing on the rainfall trend over SA using output from ten Coupled Model Intercomparison Project Phase 6 (CMIP6) models (Eyring et al., 2016), each with 3–10 ensemble members (Table S1), and calculated linear trends over the period 1945–2005. We included experiments from the Detection and Attribution Model Intercomparison Project (DAMIP; (Gillett et al., 2016)), and selected models based on the availability of historical all-forcing (hist-All), greenhouse gas–only (hist-GHG), and anthropogenic aerosol–only (hist-AER) simulations. Model agreement was assessed using a sign-consistency criterion, defined as regions where at least 70% of models agree on the direction of change. All model outputs were interpolated to a common 1.5° × 2° horizontal grid to facilitate intermodel comparison. For each model, ensemble means were first computed to reduce the influence of internal climate variability. These model means were then averaged across models to obtain the final multimodel mean (MMM). This two-step averaging approach further suppressed internal variability and provided a more robust estimate of the externally forced climate response. The MMM reproduced the spatial patterns and magnitude of climatological DJF rainfall and low-tropospheric circulation reasonably well (Figs. 1 and S2), consistent with previous studies (Li et al., 2015; Sreekala et al., 2022; Addisuu et al., 2025). Near-surface temperature anomalies were defined relative to the contemporaneous tropical ocean mean (25°S–25°N), and trends were computed from these anomaly fields. The velocity potential was derived from the horizontal wind field using a spherical harmonic decomposition. Vertically integrated moisture flux was calculated as the mass-weighted integral of specific humidity multiplied by horizontal wind from 1000 to 200 hPa, with moisture flux convergence defined as the negative divergence of the flux.

2.3 PDRMIP simulations

Simulations from the Precipitation Driver Response Model Intercomparison Project (PDRMIP) (Myhre et al., 2017) were used to corroborate the historical CMIP6 analysis. We examined experiments with step-function perturbations, including

https://doi.org/10.5194/egusphere-2026-2198
Preprint. Discussion started: 20 May 2026

a global doubling of CO_2 relative to year 2000 (Global CO_2 × 2), a fivefold increase in sulfate (Global SUL × 5), a tenfold increase in black carbon (Global BC × 10), and a tenfold increase in sulfate over Asia (10°–50° N, 60°–140° E; Asia SUL × 10). The step-function perturbations applied in PDRMIP differed from the transient evolution of real-world emissions but enabled a clearer identification of equilibrium and fast atmospheric responses to large-magnitude forcings. Model outputs were remapped to a common 1.5° × 2° horizontal grid to ensure consistency across models. Analyses were based on MMM across seven CMIP5-generation models (Table S2). Each perturbed simulation was paired with a corresponding control simulation. We analyzed the fully coupled experiments, integrated for 100 years using a fully coupled atmosphere–ocean configuration, using years 51–100. All reported responses were defined as differences between the perturbation and control experiments.

2.4 RAMIP simulations

We also used simulations from the Regional Aerosol Model Intercomparison Project (RAMIP; Wilcox et al., 2023), part of the extended CMIP6 framework (CMIP6Plus). RAMIP built upon CMIP6 historical simulations (1850–2014) and adopted SSP3–7.0 as the baseline scenario, characterized by relatively weak air-quality controls and sustained aerosol emissions. These simulations were used to isolate and quantify the climate response to regionally perturbed aerosol emissions and their influence on large-scale circulation and precipitation. Regional perturbation experiments were performed by replacing SSP3–7.0 emissions of SO_2, black carbon (BC), and organic carbon (OC) with SSP1–2.6 emissions over specific source regions. In this study, we analyzed the experiments with perturbations over EAS and SAS, allowing assessment of both individual regional influences and associated remote climate responses. RAMIP simulations spanned 2015 to at least early 2051 in a fully coupled atmosphere–ocean configuration. We focused on the final 15-year period (2035–2049), during which the perturbation experiments imposed substantial reductions in regional SO_2 emissions (approximately 20 Tg yr^{-1} over EAS and 15 Tg yr^{-1} over SAS). While the SSP scenarios prescribed reductions in aerosol emissions in both regions, the magnitude of the reduction over EAS was comparable to recent observed emission declines (Samset et al., 2025), whereas South Asian aerosol emissions have continued to increase in reality. Climate responses were defined as the difference between the perturbation experiments and the baseline simulation (SSP370-EAS126aer − SSP370 and SSP370-SAS126aer − SSP370), averaged over 2035–2049. The associated effective radiative forcing patterns, with multimodel global mean values of 0.15±0.07 W m^{-2} and 0.10±0.05 W m^{-2} respectively, are discussed in Allen et al. (2026). Output from 10 fully coupled atmosphere–ocean Earth system models, each with 10 ensemble members, was regridded to a common 1.5° × 2° horizontal resolution before analysis (Table S3).

2.5 Climate and vegetation indices

In this study, observed gross primary productivity (GPP), leaf area index (LAI), and the Fire Weather Index (FWI) were used to characterize recent changes in vegetation productivity, structure, and fire-conducive climate conditions over SA.

https://doi.org/10.5194/egusphere-2026-2198
Preprint. Discussion started: 20 May 2026

GPP was employed as a proxy for ecosystem carbon uptake. We used the FluxSat GPP dataset (FS v2.2), which provides monthly global GPP estimates derived from MODIS surface reflectance and top-of-atmosphere photosynthetically active radiation (Joiner and Yoshida, 2021) at a horizontal resolution of 0.5° × 0.625°. DJF GPP was calculated by averaging monthly values over December–February of each hydrological year.

LAI was a key vegetation structural parameter that characterized canopy density and leaf area availability. Monthly LAI was obtained from the MODIS MOD15A2 Collection 6 product (Lin et al., 2023), which was aggregated to a 0.5° × 0.5° horizontal resolution. The DJF mean LAI was used to represent canopy conditions during the austral summer.

FWI was used as an indicator of fire danger, integrating meteorological controls on potential fire intensity, including fuel dryness and fire spread. We used FWI from the GEFF–ERA5 fire danger reanalysis, derived from the Canadian Fire Weather Index System and driven by ECMWF ERA5 meteorological fields (Copernicus Climate Change Service, 2019). The annual maximum FWI was used to characterize fire-weather risk.

3 Results

3.1 Observed and simulated precipitation trends

Observational data show that DJF precipitation changes across SA during the second half of the 20th century (1945-2005) exhibit a coherent large-scale pattern (Fig. 1a), with robust features across different datasets (Fig. S3a). A significant increase in precipitation is observed across the southern part of SA (hereafter SSA; 15–34°E, 25–35°S; land only) and MDG (43–51°E, 12–26°S; land only), in contrast to drying in the northern regions of SA.

To further characterize long-term precipitation variability, Figs. 1c and 1d present the observed time series of DJF rainfall anomalies over SSA and MDG, respectively. Beyond pronounced interannual and decadal fluctuations, both records exhibit a noticeable multidecadal increase from 1945 to 2005, as also documented in previous studies (MacKellar et al., 2014; Kruger and Nxumalo, 2017). Over SSA (Fig. 1c), DJF precipitation increased by +0.28 mm d^{-1}/+0.21 mm d^{-1} in CRU/GPCC over 61 years, corresponding to 11–14% of the long-term climatological mean (1961–1990), indicating a consistent increase across datasets, albeit with limited statistical significance. Over MDG (Fig. 1d), DJF precipitation increased by +1.25 mm d^{-1}/+0.60 mm d^{-1} in CRU/GPCC over 61 years, corresponding to 7–14% of the long-term climatological mean (1961–1990); the increase is robust across datasets, and above the 90% statistical significance in CRU. All trends are calculated from the original (unfiltered) time series, while the smoothed curves are shown only to highlight low-frequency variability. Sliding-window trend analyses further demonstrate that the identified trend is robust across a wide range of start and end years (Fig. S4). Additional EOF analysis of low-pass-filtered precipitation within the domain of Fig. 1a yields the first mode exhibiting a pattern similar to that shown in Fig. 1a and explaining ~26% of the variability, with the corresponding principal component showing a positive trend over the examined period (not shown). This provides further evidence that the precipitation anomalies identified above are part of a coherent large-scale mode of variability, suggesting the influence of a consistent driving mechanism.

https://doi.org/10.5194/egusphere-2026-2198
Preprint. Discussion started: 20 May 2026

Despite its coarser resolution, the hist-All MMM captures the main spatio-temporal characteristics of the observed precipitation trends. However, amounts are smaller (Fig. 1b). The ensemble simulates enhanced oceanic rainfall south of the equator and reduced precipitation to the north, consistent with observations. In particular, the simulated rainfall pattern over South Africa and the surrounding areas aligns with observations, although the amounts are slightly underestimated. This reduced amplitude is expected, as the MMM isolates the externally forced response by averaging across ensemble members and models, thereby suppressing internal climate variability that may contribute to the observed trends. In addition, intermodel averaging across differing model responses likely further smooths spatial patterns and reduces regional contrasts (Knutti et al., 2010; Hegerl and Zwiers, 2011). The sign of the key precipitation anomalies is consistent across most of the models (at least 7 out of 10), highlighting the robustness of this meridional contrast. The hist-AER MMM closely resembles the hist-All response, exhibiting a pronounced meridional precipitation dipole over SA and the adjacent Indian Ocean, consistent with a southward displacement of the ITCZ (Fig. 2a). The aerosol-related precipitation response is also robust across most of the model ensembles (at least 7 out of 10). In contrast, the hist-GHG MMM displays a similar large-scale pattern but with the opposite sign (Fig. 2b). This follows from a GHG-induced increase in temperature and associated moistening, which amplifies existing patterns of moisture convergence and divergence, consistent with the "wet-gets-wetter, dry-gets-drier" paradigm (Held and Soden, 2006). These results suggest that aerosol forcing plays a dominant role in shaping the observed multidecadal changes in precipitation over SA. Some sub-regional discrepancies between observations and models remain, such as over parts of MDG, likely associated with unresolved fine-scale interactions between winds and complex topography (Munday et al., 2025).

https://doi.org/10.5194/egusphere-2026-2198
Preprint. Discussion started: 20 May 2026

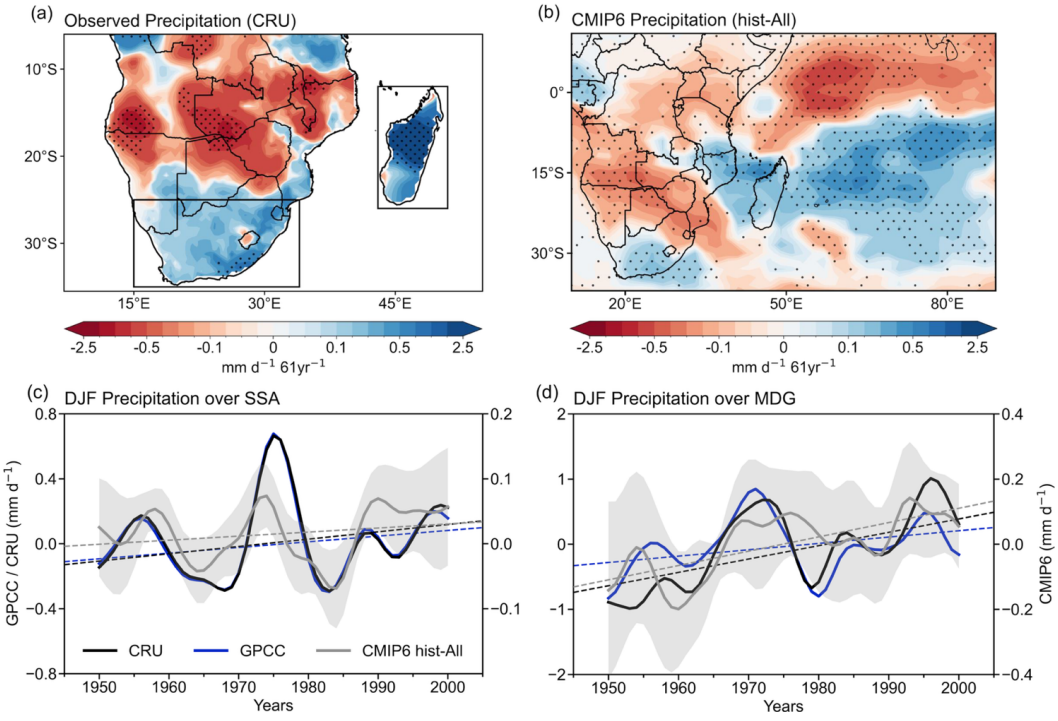

Figure 1: Spatial distribution of the 1945–2005 linear trend in DJF precipitation for (a) CRU and (b) the CMIP6 hist-All MMM. Stippling in (a) indicates statistical significance at the 90% confidence level, while stippling in (b) indicates regions where at least 70% of models agree on the sign of change. Time series of area-averaged DJF precipitation anomalies (relative to the 1961–1990 climatology) over (c) SSA (15–34°E, 25–35°S; land only) and (d) MDG (43–51°E, 12–26°S; land only). The time series are smoothed using a 10-year Lanczos low-pass filter to highlight low-frequency (multidecadal) variability. Black and blue lines represent CRU and GPCC observations, respectively, while the gray line denotes CMIP6 hist-All MMM. Gray shading indicates ±0.5 standard deviations across the 10 models. The 1945–2005 least-squares linear trends are calculated from the original (unfiltered) time series and are shown as dashed lines in the corresponding colors.

https://doi.org/10.5194/egusphere-2026-2198
Preprint. Discussion started: 20 May 2026

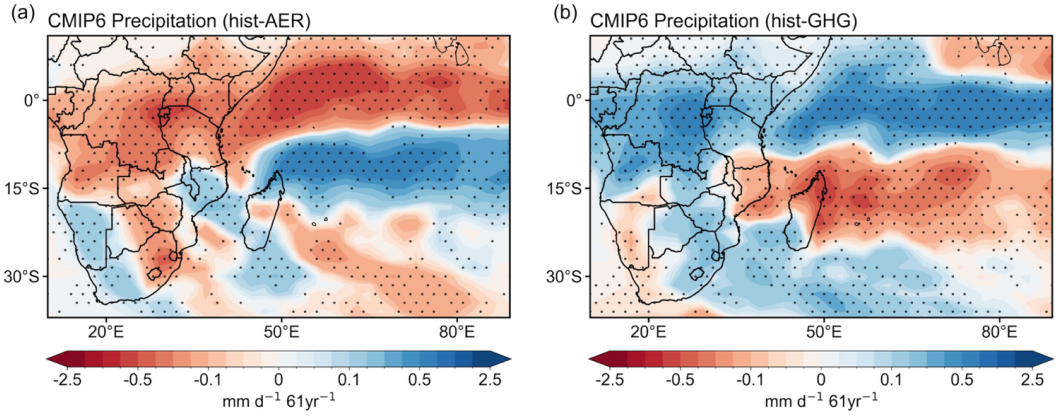

Figure 2: Spatial distribution of the 1945–2005 linear trend in DJF precipitation for the CMIP6 MMM of (a) hist-AER and (b) hist-GHG simulations. Stippling indicates regions where at least 70% of models agree on the sign of change.

3.2 Atmospheric Circulation Response to Aerosol Forcing

To provide context for the circulation and precipitation responses discussed below, we first examine the DJF climatological mean state over 1961–1990 (Fig. S2). Climatological precipitation is concentrated over central Africa and northern MDG, while relatively dry conditions prevail over SSA and southern MDG (Fig. S5c). The associated large-scale circulation is characterized by low-level easterlies over the tropical Indian Ocean and westerlies south of the equator, consistent with the mean position of the Hadley circulation and the regional monsoon system (Fig. S5d). This background circulation defines the climatological moisture transport pathways into SA.

Against this climatological background, coherent adjustments in large-scale circulation accompany the aerosol-forced precipitation response. In the CMIP6 hist-AER MMM, anthropogenic aerosols cool the Northern Hemisphere relative to the Southern Hemisphere (Fig. 3a), producing an anomalous interhemispheric temperature gradient and a southward shift of the Hadley circulation that helps compensate for the associated energy imbalance. The resulting cross-equatorial energy transport occurs primarily in the upper troposphere as dry static energy and is associated with the northward branch of the Hadley cell (Hwang et al., 2013; Liu et al., 2018). At the same time, the upper branch of the Hadley cell exhibits a southward shift (as see in the 200-hPa panel; Fig. 3b), consistent with a southward displacement of the tropical rain belt toward SA latitudes.

In addition to this hemispheric-scale adjustment, aerosols generate near-surface temperature and sea level pressure gradients across the Indian Ocean (Figs. 3a, c). Relative to the climatological state, this represents a strengthening and southward shift of the cross-equatorial flow, enhancing moisture transport into SA further to the south. A large anomalous anticyclone over South and Eastern Asia, generated by local aerosol cooling of the land as well as of the surrounding

https://doi.org/10.5194/egusphere-2026-2198
Preprint. Discussion started: 20 May 2026

oceanic areas, leads to anomalous northeasterlies over the north-equatorial Maritime Continent and the eastern Indian Ocean. The flow turns to north-westerlies after crossing the equator because of the Coriolis effect, resulting in marked south-equatorial westerlies across the Indian Ocean. In the Southern Hemisphere, in addition to the overall weaker oceanic cooling (relative warming) compared to the Northern regions and the widespread ascent, a negative Indian Ocean Dipole-like pattern emerges, with enhanced sea surface warming and ascent in the eastern subtropical basin compared to the western part. This zonal gradient, albeit secondary to the mean aerosol-induced meridional shift, enhances moisture transport from the tropical Indian Ocean toward southern Africa and intensifies moisture convergence over SSA and MDG, while relative drying occurs over the tropical regions to the north of SA. Interactions between the prevailing southeasterlies and local topographical features, and the induced low-level divergent flow (e.g., over eastern South Africa), help explain the presence of localized land drying (Fig. 3d).

The close correspondence between precipitation, moisture fluxes, and circulation trends in hist-All and hist-AER indicates that anthropogenic aerosols play a dominant role in shaping the forced component of historical Indo–southwestern Indian Ocean hydroclimate variability via changes in wind patterns (Figs. 3 and S5, which shows the equivalent of Fig. 3 for hist-All).

To assess the potential role of Asian aerosols in driving this circulation–precipitation linkage further, we analyze idealized PDRMIP perturbation experiments (Figs. 4 and S6). The global $CO_2 \times 2$ and BC × 10 experiments do not reproduce the characteristic Indian Ocean meridional precipitation dipole seen in hist-All (Figs. S6a, b). Global sulfate forcing (SUL × 5) produces a hemispheric-scale precipitation response characterized by a southward displacement of the ITCZ (Fig. 4a), consistent with an aerosol-induced interhemispheric temperature gradient. This large-scale adjustment is accompanied by consistent sea level pressure anomalies and circulation changes over the Indo–Pacific region, featuring a northward pressure gradient and anomalous near-equatorial westerlies (Fig. 4c). However, despite the meridional shift of the tropical rain belt, the precipitation response over SSA and MDG exhibits a more widespread drying tendency compared to hist-All associated to a more pronounced anomalous anticyclone. By contrast, the Asian sulfate perturbation (Asia SUL × 10) shows strong agreement with the CMIP6 hist-All and hist-AER patterns, producing a pronounced cross-equatorial pressure gradient, a strengthened and southward-shifted monsoonal westerly flow (Fig. 4d), and an Indian Ocean meridional precipitation dipole accompanied by increased rainfall over SA (Fig. 4b). The response pattern is robust across different PDRMIP models and, in particular, does not depend on the specific aerosol prescription methodology (i.e., emissions versus concentrations). Together, the CMIP6 circulation diagnostics and the targeted PDRMIP experiments provide consistent evidence that changes in Asian sulfate aerosols are associated with southern African rainfall anomalies through large-scale circulation adjustments over the Indo–western Pacific region.

Overall, these results indicate that the southern African precipitation response to Asian sulfate forcing is primarily mediated by ocean–atmosphere coupling rather than fast atmospheric adjustments. In the coupled simulations, enhanced Asian sulfate emissions cool the Northern Hemisphere relative to the Southern Hemisphere, generating an interhemispheric

https://doi.org/10.5194/egusphere-2026-2198
Preprint. Discussion started: 20 May 2026

311 energy imbalance that alters Indian Ocean SST. The resulting hemispheric temperature contrast strengthens the cross-
312 equatorial sea level pressure gradient and shifts the Hadley circulation and associated monsoonal westerlies southward.
313 The associated Indian Ocean SST anomalies induce a zonal gradient and strengthen cross-equatorial flow, enhancing
314 moisture transport and convergence over SSA while promoting drying to the north of SA.

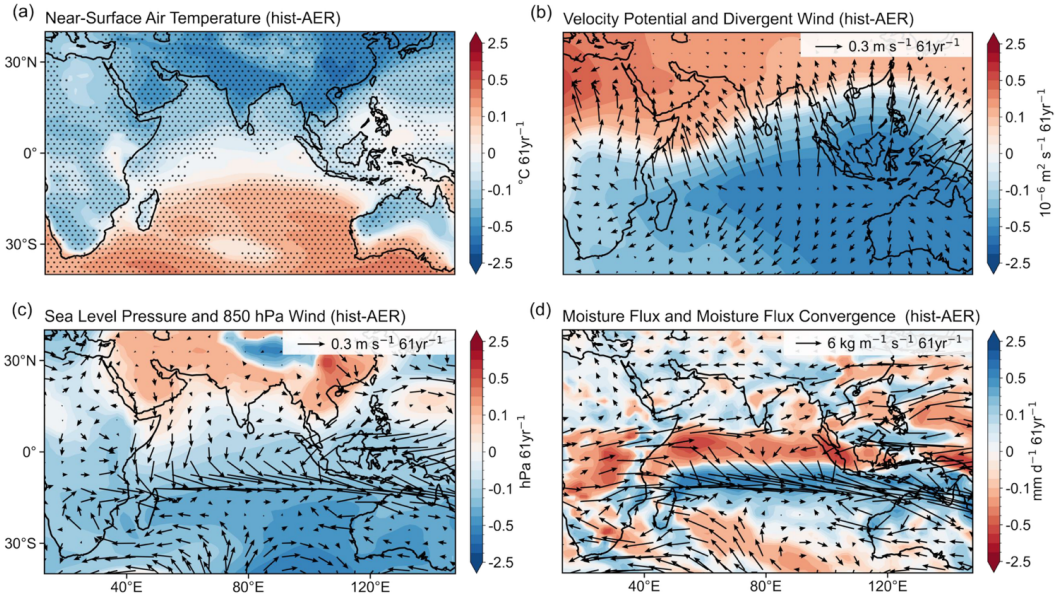

315

316 **Figure 3: Spatial distribution of trends over 1945–2005 for DJF: (a) near-surface temperature relative to the contemporaneous**
317 **tropical ocean mean (25°S–25°N), (b) velocity potential (shading) with divergent wind (vectors) at 200 hPa, (c) mean sea level**
318 **pressure (shading) with 850 hPa winds (vectors), and (d) vertically integrated moisture flux (vectors) and moisture flux**
319 **convergence (shading) for the hist-AER simulations. All trends are based on the MMM across 10 CMIP6 models. Stippling**
320 **indicates regions where at least 70% of the models agree on the sign of change.**

321

https://doi.org/10.5194/egusphere-2026-2198
Preprint. Discussion started: 20 May 2026

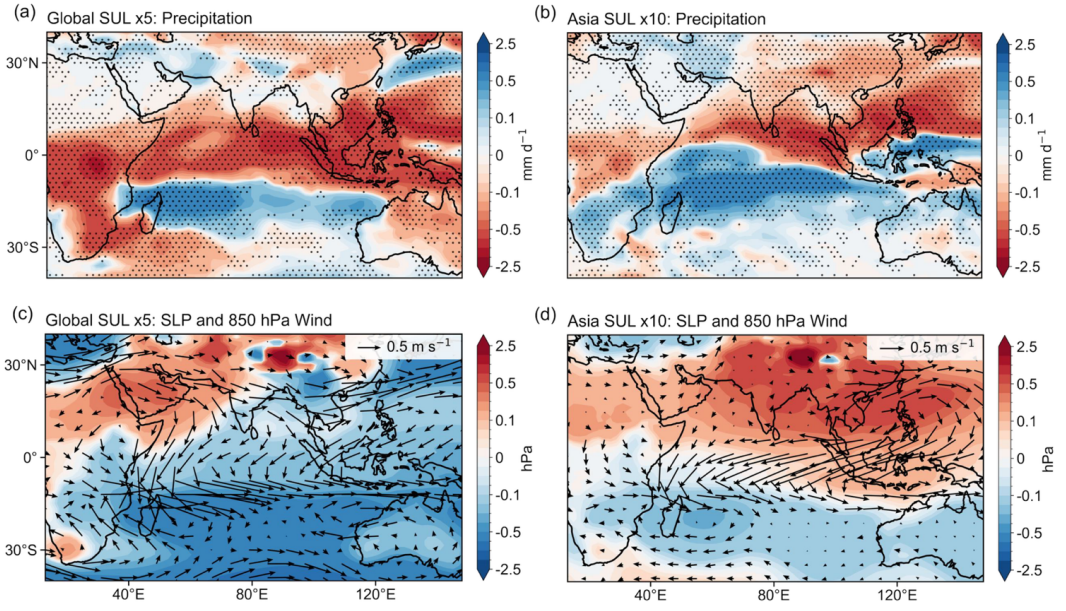

Figure 4: Spatial anomalies during DJF in (a, b) precipitation, (c, d) mean sea level pressure (colour) with 850-hPa winds (vectors) for the total equilibrium response in the (left) Global SUL×5, and (right) Asia SUL×10 simulations from PDRMIP. Seven models were used to calculate the MMM, and stippling indicates regions where at least 70% of the models agree on the sign of change.

3.3 Mid-2000s hydroclimatic reversal and ecosystem responses

Since the mid-2000s, anthropogenic aerosol emissions over EAS have declined rapidly (Hoesly et al., 2018; McDuffie et al., 2020). Over the same period (2006–2020), DJF precipitation shows a widespread drying signal across much of SA (Fig. 5a). For this period, we primarily rely on the TAMSAT rainfall dataset (Fig. 5a; Fig. S3), as gauge-based products such as CRU and GPCC suffer from substantially reduced station coverage over central Africa after 2000, leading to increased uncertainties (Becker et al., 2013; Harris et al., 2020). In contrast, TAMSAT, which is primarily based on satellite observations, provides more spatially complete and temporally consistent estimates over Africa, making it particularly suitable for analyzing recent hydroclimatic changes (i.e., post-2000s). Over regions with relatively dense station coverage, such as South Africa, TAMSAT shows good agreement with gauge-based datasets, supporting its reliability. This provides confidence in its representation of drying patterns over data-sparse regions such as central Africa. Interestingly, the rainfall trend during 2006–2020 exhibits a spatial pattern broadly similar to that during 1945–2005, but with the opposite sign, and with a larger magnitude.

This hydroclimatic shift is accompanied by pronounced ecosystem responses (Figs. 5b–d). During 2006–2020, both GPP

https://doi.org/10.5194/egusphere-2026-2198
Preprint. Discussion started: 20 May 2026

and LAI decline over large parts of SA, while increases are observed over parts of central Africa (Figs. 5b, c). These changes are consistent with reduced soil moisture availability and enhanced plant water stress under drier conditions (Zhou et al., 2021; Feldman et al., 2024a). Concurrently, the FWI increases across much of the region (Fig. 5d), particularly in areas experiencing pronounced drying, indicating more favorable atmospheric conditions for wildfire occurrence and spread (Abatzoglou and Williams, 2016; Jain et al., 2022; Ribeiro et al., 2022). Note that while we do not quantify the specific contribution of rainfall deficits to these trends, which may also reflect concurrent changes in temperature, humidity, and wind speed, rainfall deficits are widely recognized as a primary driver of vegetation dryness and wildfire risk in the tropics (Brando et al., 2014; Wimberly et al., 2024).

To assess whether the observed hydroclimatic reversal is dynamically consistent with aerosol-driven circulation adjustments, we analyze the RAMIP regional aerosol perturbation experiments over EAS. The EAS reduction experiment produces a clear Indo–western Pacific meridional precipitation dipole (Fig. 6), with enhanced rainfall over the equatorial Indian Ocean and reduced precipitation over the southern Indian Ocean and SA. This pattern closely resembles the observed post–mid-2000s drying over SA (Fig. 5a). This agreement suggests that reductions in East Asian anthropogenic aerosol emissions can induce large-scale circulation adjustments that favor drying over southern Africa. Taken together with the observed temporal correspondence and ecosystem responses, these results provide strong evidence that East Asian aerosols have played an important role in the recent hydroclimatic changes over the region.

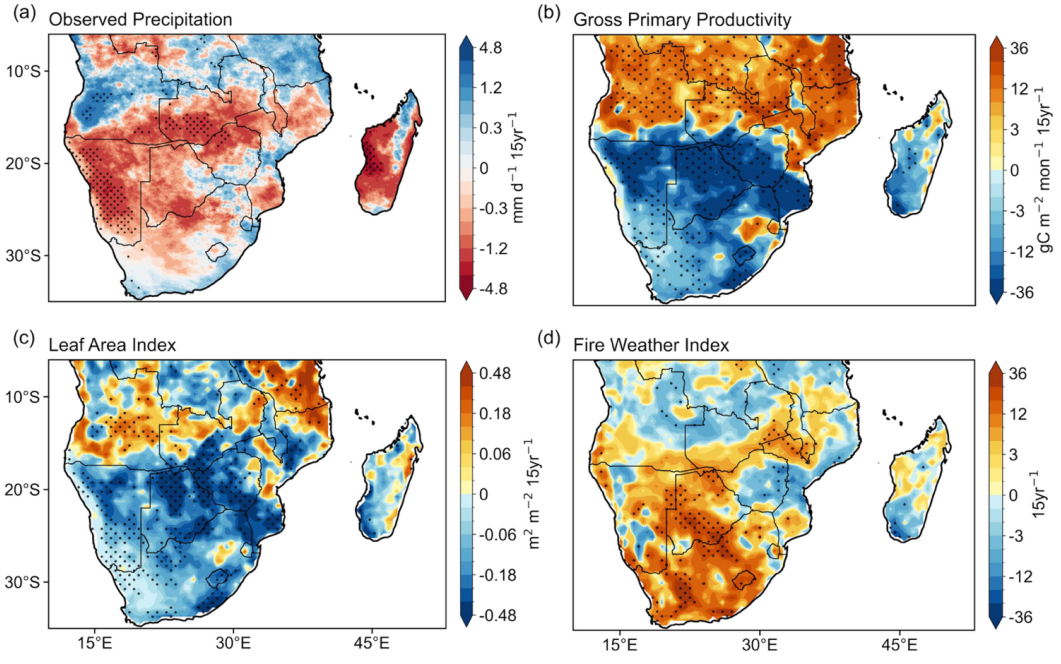

Figure 5: Spatial distribution of trends over 2006–2020 for (a) observed DJF precipitation from TAMSAT, (b) DJF mean GPP, (c) DJF mean LAI, and (d) annual maximum FWI. Stippling indicates statistical significance at the 90% confidence level.

https://doi.org/10.5194/egusphere-2026-2198
Preprint. Discussion started: 20 May 2026

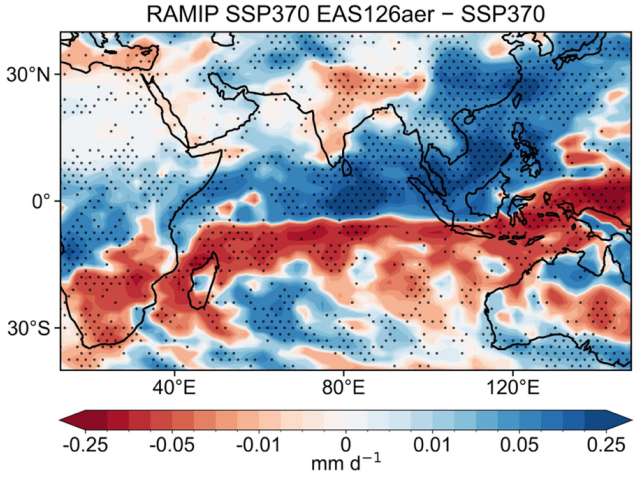

Figure 6: Spatial distribution of the DJF mean over 2035–2049 for precipitation from the RAMIP simulations. Results are shown as the MMM across 10 models (100 ensemble members) and are defined as the difference between the East Asian perturbation (SSP370-EAS126aer) and the baseline simulation (SSP370). Stippling indicates regions where at least 70% of models agree on the sign of change.

4 Discussion and Conclusions

This study investigates the influence of anthropogenic aerosol forcing from EAS on austral summer (DJF) rainfall over SA on multidecadal timescales. Observations reveal a meridional contrast, with a persistent decline in precipitation over the northern part of SA and adjacent tropical regions, alongside increased rainfall across SSA, MDG, and the adjacent southern Indian Ocean during 1945–2005, followed by a reversal of these trends over 2006–2020. The timing of the reversal coincides with the rapid decline in East Asian aerosol emissions since the mid-2000s.

CMIP6 single-forcing simulations indicate that anthropogenic aerosols account for a substantial fraction of the forced precipitation response over the southwestern Indian Ocean. The hist-AER ensemble reproduces the observed meridional precipitation dipole, with increased rainfall over SSA, MDG, and the adjacent southern Indian Ocean, and concurrent drying over the northern part of SA and the adjacent tropical ocean, whereas hist-GHG simulations produce an opposing response. The aerosol-forced signal is associated with coherent circulation adjustments, including an anomalous interhemispheric temperature gradient induced by Northern Hemisphere cooling and a consequent southward displacement of the Hadley circulation. The resulting circulation changes strengthen low-level westerlies and enhance moisture transport from the adjacent tropical oceans into SA, leading to increased low-level moisture convergence and enhanced precipitation over SSA, MDG and the adjacent southern Indian Ocean, alongside concurrent drying over the northern part of SA and the adjacent tropical ocean. Idealized PDRMIP experiments corroborate the above findings on the role of aerosols, and also

https://doi.org/10.5194/egusphere-2026-2198
Preprint. Discussion started: 20 May 2026

further help to gain insights into the nature of the forcing. Global CO_2 and black carbon perturbations do not reproduce the key Indian Ocean–southern African precipitation structure. In contrast, the regional Asian sulfate perturbation produces circulation and precipitation responses that closely resemble those of the CMIP6 historical simulations.

The observed post mid-2000s changes exhibit a reversal of the earlier meridional precipitation dipole, with drying over SSA and MDG and concurrent wetting over the northern part of SA. These hydroclimatic changes are accompanied by coherent land–ecosystem responses. During 2006–2020, decreases in GPP and LAI occur alongside the drying signal, and FWI increases over large parts of the region, consistent with drier fuel conditions and more fire-favorable meteorology. These concurrent changes suggest that the hydroclimatic reversal is reflected not only in rainfall but also in ecosystem functioning and fire-weather risk.

RAMIP experiments further demonstrate that changes in Asian aerosol emissions, particularly reductions over EAS, can produce a meridional precipitation dipole over the Indo–western Pacific. The response features reduced rainfall over the southern Indian Ocean and SA and enhanced rainfall closer to the equatorial Indian Ocean. This projected pattern closely resembles the observed post–mid-2000s changes, supporting the interpretation that recent and ongoing aerosol reductions in EAS can contribute to drying over the southwestern Indian Ocean region by altering large-scale circulation. A key question is whether South Asian aerosols contribute to the recent changes, which is plausible given their proximity to the analysed region. However, aerosol changes over SAS are much smaller and produce an opposite precipitation response, suggesting a limited contribution to the observed drying (Fig. S7). Together, these results highlight the dominant role of East Asian aerosol reductions in driving the recent hydroclimatic reversal over SA.

An important consideration is the extent to which SST, particularly over the Indian Ocean, contributed to shaping the aerosol signal discussed above. While the hist-All ensemble exhibits widespread warming across the Indian Ocean, this warming is most pronounced over the western and central south-equatorial basin, with weaker temperature increases (relative cooling) north of 10°N across parts of the Arabian Sea, the Bay of Bengal, and the South China Sea, as well as around 30°S. Similar patterns have been reported in previous studies over slightly different periods (Yoo et al., 2006; Jeong et al., 2022). In contrast, aerosol-induced SST trends show widespread cooling across the basin, with pronounced negative temperature anomalies north of 10°N, associated with radiation dimming from increased aerosol loading. As a result, SSTs display a clear cross-equatorial southward meridional gradient in the central and eastern basin in both hist-All and hist-AER. This gradient contributes to the development of a cross-equatorial meridional pressure gradient and the associated northeasterly-to-northwesterly low-level winds. While SST changes over the central and eastern Indian Ocean in hist-All are broadly consistent with the pattern expected from aerosol forcing, the warming in the western north-equatorial Indian Ocean and the overlying northwestward low-level flow appear more consistent with GHG forcing. These features are likely driven by enhanced warming and related thermally induced anomalous large-scale cyclonic circulation over the Arabian Peninsula.

https://doi.org/10.5194/egusphere-2026-2198
Preprint. Discussion started: 20 May 2026

We acknowledge several limitations of this study. First, the magnitude of the observed austral summer precipitation trend over SA during 1945–2005 is underestimated in the CMIP6 MMM, although most models capture the correct sign of change. The presence of individual model realizations that reproduce the observed amplitude suggests that the historical trend likely reflects a combination of anthropogenic aerosol forcing and internal climate variability. This reduced amplitude is expected, as multimodel and multi-member averaging suppresses internal climate variability, which can contribute substantially to the observed trend. In addition, observational uncertainties remain, particularly over central Africa where rain gauge coverage is sparse and has declined substantially in recent decades, increasing uncertainty in gridded precipitation products (Becker et al., 2013; Harris et al., 2020). Second, our analysis focuses on the role of East Asian anthropogenic aerosols, motivated by their dominant contribution to global aerosol emissions during the late 20th century and their marked opposite trends during the last few decades (Hoesly et al., 2018; McDuffie et al., 2020). As a result, regional forcing factors within and around Africa, including land use change and biomass burning emissions, are not considered here. Biomass burning and SO_2 emissions have also undergone substantial changes over the same period and have been shown to influence regional precipitation patterns (Hodnebrog et al., 2016; Shikwambana et al., 2020), and may therefore contribute to the observed hydroclimatic variability over SA. Finally, inherent uncertainties in simulating aerosol radiative effects remain a challenge. The representation of aerosol–cloud interactions is a well-known source of diversity among CMIP6 models, which can lead to variations in the simulated magnitude of the interhemispheric temperature gradient and the resulting sensitivity of the ITCZ shift (Bellouin et al., 2020; Smith et al., 2020).

Our results improve the understanding of how East Asian anthropogenic aerosols influence rainfall variability over SA and the associated dynamical mechanisms. Reducing uncertainties in future rainfall projections under evolving aerosol emission trajectories remains an important challenge, particularly for informing adaptation strategies in regions vulnerable to hydroclimatic change (Li et al., 2017; Samset et al., 2019). Future work could further examine how aerosol forcing modulates intra-seasonal rainfall variability and seasonal characteristics, including rainfall onset, duration, and dry spells. These processes are particularly relevant given emerging ecosystem stresses across SA, including increasing wildfire activity, shifts in vegetation productivity, and growing vulnerability of rain-fed agricultural systems. Climate change and shifting precipitation patterns may also affect biodiversity-rich ecosystems in SA, where rainfall variability strongly influences vegetation dynamics and drought stress, potentially threatening ecosystem stability, particularly in the northern forest and savanna regions (Hannah et al., 2008; Sintayehu, 2018).

Data availability

GPCC data are available at https://opendata.dwd.de/climate_environment/GPCC/html/. CRU data are available at https://crudata.uea.ac.uk/cru/data/hrg/. TAMSAT data are available at https://research.reading.ac.uk/tamsat/. GPCP and CMAP data are available at https://psl.noaa.gov/data/gridded/data.gpcp.html and https://psl.noaa.gov/data/gridded/data.cmap.html. ERA5 data are available at https://cds.climate.copernicus.eu/. PDRMIP model data are available at https://www.wdc-climate.de/ui/. RAMIP model data are available at

https://doi.org/10.5194/egusphere-2026-2198
Preprint. Discussion started: 20 May 2026

https://catalogue.ceda.ac.uk/uuid/4680fd74cf2244ba8476ed2617e3b41f/. LAI data are available at http://globalchange.bnu.edu.cn/research/data. GPP data are available at https://disc.gsfc.nasa.gov/. FWI data are available at https://ewds.climate.copernicus.eu/. CEDS emissions data are available at https://zenodo.org/records/15059443.

Author contribution

BS and MAB designed the study. BS performed the analysis, processed the data, and completed the first draft of the manuscript. HW and LJW assisted with the analysis. BS and MAB discussed the results and edited the manuscript. ASG, LJW, TPSR, CTSB, QL, PN, RJA, BHS, JM, GGP, TT, KT, SA, MTE, KVS, and DMW provided suggestions on the analysis and interpretation of the results.

Competing interests

At least one of the (co-)authors is a member of the editorial board of Atmospheric Chemistry and Physics. The authors declare that they have no other competing interests.

Acknowledgements

We are grateful to colleagues who provided valuable feedback during the development of this study. We acknowledge the World Climate Research Programme, which, through its Working Group on Coupled Modelling, coordinated and promoted CMIP6. We thank the climate modelling groups for producing and making available their model output, the Earth System Grid Federation (ESGF) for archiving the data and providing access, and the multiple funding agencies who support CMIP6 and ESGF. We acknowledge the use of the JASMIN super-data cluster (Lawrence et al., 2012), managed by the UK Science and Technology Facilities Council (STFC) Centre for Environmental Data Analysis (CEDA), for part of the data processing and analysis. We acknowledge the contributions of all project partners involved in data provision and discussions. We gratefully acknowledge the contributors to the Regional Aerosol Model Intercomparison Project (RAMIP) simulations used in this study, including, among others, Paul Kushner, Neil Swart, Luke Fraser-Leach, Larissa Nazarenko, David Paynter, Declan O'Donnell, Risto Makkonen, Annica M. L. Ekman, Anna Lewinschal, Steven T. Rumbold, James Keeble, Paul Griffiths, and Molly MacRae.

Financial support

We acknowledge support from the UK International Development from the Foreign, Commonwealth and Development Office REDAA BResilient project grant RGC2PGS2FP-10001 (BS, MAB, AG, CB, TR), the Natural Environment Research Council (NERC) grant TerraFIRMA NE/W004895/1 (LJW, PTG, STR), the Research Council of Norway grant 324182 (CATHY; BHS, LJW, RJA); Horizon Europe grant 101137639 (CleanCloud; BHS, LJW), the National Center for Atmospheric Science, UK (LJW, STR), the US National Oceanic and Atmospheric Administration award NA23OAR4310601 (GP), the US National Science Foundation grant AGS-2153486 (RJA), and the University of Reading

https://doi.org/10.5194/egusphere-2026-2198
Preprint. Discussion started: 20 May 2026

Advancing the Frontiers of Earth System Prediction (AFESP) Programme award number A3720200 (SA), the Environment Research and Technology Development Fund grant JPMEERF20232001 and JPMEERF20262002 of the Environmental Restoration and Conservation Agency provided by the Ministry of the Environment of Japan (NO), the Arctic Challenge for Sustainability 3 (ArCS-3) grant JPMXD1720251001 (NO), and the Global Environmental Research Coordination System grant from the Ministry of the Environment of Japan grant MLIT2253 (NO).

References

Abatzoglou, J. T. and Williams, A. P.: Impact of anthropogenic climate change on wildfire across western US forests, Proceedings of the National Academy of Sciences, 113, 11770–11775, 10.1073/pnas.1607171113, 2016.

Addisuu, A. A., Mengistu Tsidu, G., and Basupi, L. V.: Improving Daily CMIP6 Precipitation in Southern Africa Through Bias Correction—Part 1: Spatiotemporal Characteristics, 10.3390/cli13050095, 2025.

Adler, R. F., Huffman, G. J., Chang, A., Ferraro, R., Xie, P.-P., Janowiak, J., Rudolf, B., Schneider, U., Curtis, S., Bolvin, D., Gruber, A., Susskind, J., Arkin, P., and Nelkin, E.: The Version-2 Global Precipitation Climatology Project (GPCP) Monthly Precipitation Analysis (1979–Present), Journal of Hydrometeorology, 4, 1147–1167, https://doi.org/10.1175/1525-7541(2003)004<1147:TVGPCP>2.0.CO;2, 2003.

Agossou, C. and Kang, S.: Climatic factors controlling interannual variability of the onset of vegetation phenology in the northern Sub-Saharan Africa from 1988 to 2013, African Journal of Ecology, 58, 299–308, 10.1111/aje.12699, 2020.

Albrecht, B. A.: Aerosols, Cloud Microphysics, and Fractional Cloudiness, Science, 245, 1227–1230, 10.1126/science.245.4923.1227, 1989.

Allen, R. J.: A 21st century northward tropical precipitation shift caused by future anthropogenic aerosol reductions, Journal of Geophysical Research: Atmospheres, 120, 9087–9102, 10.1002/2015JD023623, 2015.

Allen, R. J., Wilcox, L. J., Samset, B. H., Ahmadi, S., Ekman, A. M. L., Elling, M. T., Fraser-Leach, L., Griffiths, P., Keeble, J., Koshiro, T., Kushner, P., Lewinschal, A., MacRae, M., Makkonen, R., Merikanto, J., Nabat, P., Nazarenko, L., O'Donnell, D., Oshima, N., Paynter, D., Persad, G., Rumbold, S. T., Swart, N., Takemura, T., Tsigaridis, K., von Salzen, K., and Westervelt, D. M.: Decomposing the global and regional aerosol effective radiative forcing associated with strong versus weak air quality policies by Mid-21st century, Environ. Res.: Climate, 5, 025014, 10.1088/2752-5295/ae5418, 2026.

Andrews, T. and Forster, P. M.: Energy budget constraints on historical radiative forcing, Nat. Clim. Chang., 10, 313–316, 10.1038/s41558-020-0696-1, 2020.

Ansah, E. W., Amoadu, M., Obeng, P., and Sarfo, J. O.: Climate change, urban vulnerabilities and adaptation in Africa: a scoping review, Climatic Change, 177, 71, 10.1007/s10584-024-03711-8, 2024.

Ashfaq, M., Cavazos, T., Reboita, M. S., Torres-Alavez, J. A., Im, E.-S., Olusegun, C. F., Alves, L., Key, K., Adeniyi, M. O., Tall, M., Sylla, M. B., Mehmood, S., Zafar, Q., Das, S., Diallo, I., Coppola, E., and Giorgi, F.: Robust late twenty-first century shift in the regional monsoons in RegCM-CORDEX simulations, Clim Dyn, 57, 1463–1488, 10.1007/s00382-020-05306-2, 2021.

Barimalala, R., Blamey, R. C., Desbiolles, F., and Reason, C. J. C.: Variability in the Mozambique Channel Trough and Impacts on Southeast African Rainfall, Journal of Climate, 33, 749–765, 10.1175/JCLI-D-19-

https://doi.org/10.5194/egusphere-2026-2198
Preprint. Discussion started: 20 May 2026

0267.1, 2020.

Bartzke, G. S., Ogutu, J. O., Mukhopadhyay, S., Mtui, D., Dublin, H. T., and Piepho, H.-P.: Rainfall trends and variation in the Maasai Mara ecosystem and their implications for animal population and biodiversity dynamics, PLOS ONE, 13, e0202814, 10.1371/journal.pone.0202814, 2018.

Becker, A., Finger, P., Meyer-Christoffer, A., Rudolf, B., Schamm, K., Schneider, U., and Ziese, M.: A description of the global land-surface precipitation data products of the Global Precipitation Climatology Centre with sample applications including centennial (trend) analysis from 1901–present, Earth Syst. Sci. Data, 5, 71–99, 10.5194/essd-5-71-2013, 2013.

Bedeke, S. B.: Climate change vulnerability and adaptation of crop producers in sub-Saharan Africa: a review on concepts, approaches and methods, Environment, Development and Sustainability, 25, 1017–1051, 10.1007/s10668-022-02118-8, 2023.

Bellouin, N., Quaas, J., Gryspeerdt, E., Kinne, S., Stier, P., Watson-Parris, D., Boucher, O., Carslaw, K. S., Christensen, M., Daniau, A. L., Dufresne, J. L., Feingold, G., Fiedler, S., Forster, P., Gettelman, A., Haywood, J. M., Lohmann, U., Malavelle, F., Mauritsen, T., McCoy, D. T., Myhre, G., Mülmenstädt, J., Neubauer, D., Possner, A., Rugenstein, M., Sato, Y., Schulz, M., Schwartz, S. E., Sourdeval, O., Storelvmo, T., Toll, V., Winker, D., and Stevens, B.: Bounding Global Aerosol Radiative Forcing of Climate Change, Reviews of Geophysics, 58, e2019RG000660, https://doi.org/10.1029/2019RG000660, 2020.

Bollasina, M. A., Ming, Y., and Ramaswamy, V.: Anthropogenic Aerosols and the Weakening of the South Asian Summer Monsoon, Science, 334, 502–505, 10.1126/science.1204994, 2011.

Brando, P. M., Balch, J. K., Nepstad, D. C., Morton, D. C., Putz, F. E., Coe, M. T., Silvério, D., Macedo, M. N., Davidson, E. A., Nóbrega, C. C., Alencar, A., and Soares-Filho, B. S.: Abrupt increases in Amazonian tree mortality due to drought–fire interactions, Proceedings of the National Academy of Sciences, 111, 6347–6352, 10.1073/pnas.1305499111, 2014.

Cai, W., Reason, C., Mohino, E., Rodríguez-Fonseca, B., Malherbe, J., Santoso, A., Li, X., Chikoore, H., Nnamchi, H., McPhaden, M. J., Keenlyside, N., Taschetto, A. S., Wu, L., Ng, B., Liu, Y., Geng, T., Yang, K., Wang, G., Jia, F., Lin, X., Li, S., Yang, Y., Wang, J., Zhang, L., Li, Z., Wilfried, P., Zhou, L., Zhang, X., Engelbrecht, F., Li, Z., and Mutemi, J. N.: Climate impacts of the El Niño–Southern Oscillation in Africa, Nature Reviews Earth & Environment, 6, 503–520, 10.1038/s43017-025-00705-7, 2025.

Copernicus Climate Change Service: Fire danger indices historical data from the Copernicus Emergency Management Service. ECMWF [dataset], 2019.

Eyring, V., Bony, S., Meehl, G. A., Senior, C. A., Stevens, B., Stouffer, R. J., and Taylor, K. E.: Overview of the Coupled Model Intercomparison Project Phase 6 (CMIP6) experimental design and organization, Geosci. Model Dev., 9, 1937–1958, 10.5194/gmd-9-1937-2016, 2016.

Fahrenbach, N. L. S., Bollasina, M. A., Samset, B. H., Cowan, T., and Ekman, A. M. L.: Asian Anthropogenic Aerosol Forcing Played a Key Role in the Multidecadal Increase in Australian Summer Monsoon Rainfall, Journal of Climate, 37, 895–911, 10.1175/JCLI-D-23-0313.1, 2024.

Feldman, A. F., Feng, X., Felton, A. J., Konings, A. G., Knapp, A. K., Biederman, J. A., and Poulter, B.: Plant responses to changing rainfall frequency and intensity, Nature Reviews Earth & Environment, 5, 276–294, 10.1038/s43017-024-00534-0, 2024a.

Feldman, A. F., Konings, A. G., Gentine, P., Cattry, M., Wang, L., Smith, W. K., Biederman, J. A., Chatterjee, A., Joiner, J., and Poulter, B.: Large global-scale vegetation sensitivity to daily rainfall variability, Nature, 636, 380–384, 10.1038/s41586-024-08232-z, 2024b.

Gampe, D., Zscheischler, J., Reichstein, M., O'Sullivan, M., Smith, W. K., Sitch, S., and Buermann, W.: Increasing impact of warm droughts on northern ecosystem productivity over recent decades, Nat. Clim.

https://doi.org/10.5194/egusphere-2026-2198
Preprint. Discussion started: 20 May 2026

562 Chang., 11, 772–779, 10.1038/s41558-021-01112-8, 2021.
563 Gao, J., Yang, Y., Wang, H., Wang, P., and Liao, H.: Dry and warm conditions in Australia exacerbated by
564 aerosol reduction in China, Atmospheric Chemistry and Physics, 25, 10949–10964, 10.5194/acp-25-
565 10949-2025, 2025.
566 Georganos, S., Grippa, T., Vanhuysse, S., Lennert, M., Shimoni, M., Kalogirou, S., and Wolff, E.: Less is more:
567 optimizing classification performance through feature selection in a very-high-resolution remote sensing
568 object-based urban application, GIScience & Remote Sensing, 55, 221–242,
569 10.1080/15481603.2017.1408892, 2018.
570 Gillett, N. P., Shiogama, H., Funke, B., Hegerl, G., Knutti, R., Matthes, K., Santer, B. D., Stone, D., and Tebaldi,
571 C.: The Detection and Attribution Model Intercomparison Project (DAMIP v1.0) contribution to CMIP6,
572 Geosci. Model Dev., 9, 3685–3697, 10.5194/gmd-9-3685-2016, 2016.
573 Hannah, L., Dave, R., Lowry, P. P., II, Andelman, S., Andrianarisata, M., Andriamaro, L., Cameron, A., Hijmans,
574 R., Kremen, C., MacKinnon, J., Randrianasolo, H. H., Andriambololonera, S., Razafimpahanana, A.,
575 Randriamahazo, H., Randrianarisoa, J., Razafinjatovo, P., Raxworthy, C., Schatz, G. E., Tadross, M., and
576 Wilmé, L.: Climate change adaptation for conservation in Madagascar, Biology Letters, 4, 590–594,
577 10.1098/rsbl.2008.0270, 2008.
578 Harris, I., Osborn, T. J., Jones, P., and Lister, D.: Version 4 of the CRU TS monthly high-resolution gridded
579 multivariate climate dataset, Scientific Data, 7, 109, 10.1038/s41597-020-0453-3, 2020.
580 Hegerl, G. and Zwiers, F.: Use of models in detection and attribution of climate change, WIREs Climate Change,
581 2, 570–591, https://doi.org/10.1002/wcc.121, 2011.
582 Held, I. M. and Soden, B. J.: Robust Responses of the Hydrological Cycle to Global Warming, Journal of
583 Climate, 19, 5686–5699, https://doi.org/10.1175/JCLI3990.1, 2006.
584 Hersbach, H., Bell, B., Berrisford, P., Hirahara, S., Horányi, A., Muñoz-Sabater, J., Nicolas, J., Peubey, C., Radu,
585 R., Schepers, D., Simmons, A., Soci, C., Abdalla, S., Abellan, X., Balsamo, G., Bechtold, P., Biavati, G.,
586 Bidlot, J., Bonavita, M., De Chiara, G., Dahlgren, P., Dee, D., Diamantakis, M., Dragani, R., Flemming,
587 J., Forbes, R., Fuentes, M., Geer, A., Haimberger, L., Healy, S., Hogan, R. J., Hólm, E., Janisková, M.,
588 Keeley, S., Laloyaux, P., Lopez, P., Lupu, C., Radnoti, G., de Rosnay, P., Rozum, I., Vamborg, F., Villaume,
589 S., and Thépaut, J.-N.: The ERA5 global reanalysis, Quarterly Journal of the Royal Meteorological Society,
590 146, 1999–2049, https://doi.org/10.1002/qj.3803, 2020.
591 Hirasawa, H., Kushner, P. J., Sigmond, M., Fyfe, J., and Deser, C.: Evolving Sahel Rainfall Response to
592 Anthropogenic Aerosols Driven by Shifting Regional Oceanic and Emission Influences, Journal of Climate,
593 35, 3181–3193, 10.1175/JCLI-D-21-0795.1, 2022.
594 Hodnebrog, Ø., Myhre, G., Forster, P. M., Sillmann, J., and Samset, B. H.: Local biomass burning is a dominant
595 cause of the observed precipitation reduction in southern Africa, Nature Communications, 7, 11236,
596 10.1038/ncomms11236, 2016.
597 Hoesly, R. M., Smith, S. J., Feng, L., Klimont, Z., Janssens-Maenhout, G., Pitkanen, T., Seibert, J. J., Vu, L.,
598 Andres, R. J., Bolt, R. M., Bond, T. C., Dawidowski, L., Kholod, N., Kurokawa, J.-i., Li, M., Liu, L., Lu,
599 Z., Moura, M. C. P., O'Rourke, P. R., and Zhang, Q.: Historical (1750–2014) anthropogenic emissions of
600 reactive gases and aerosols from the Community Emissions Data System (CEDS), Geoscientific Model
601 Development, 11, 369–408, 10.5194/gmd-11-369-2018, 2018.
602 Humphrey, V., Berg, A., Ciais, P., Gentine, P., Jung, M., Reichstein, M., Seneviratne, S. I., and Frankenberg, C.:
603 Soil moisture–atmosphere feedback dominates land carbon uptake variability, Nature, 592, 65–69,
604 10.1038/s41586-021-03325-5, 2021.
605 Hwang, Y.-T., Frierson, D. M. W., and Kang, S. M.: Anthropogenic sulfate aerosol and the southward shift of

https://doi.org/10.5194/egusphere-2026-2198
Preprint. Discussion started: 20 May 2026

tropical precipitation in the late 20th century, Geophysical Research Letters, 40, 2845–2850, https://doi.org/10.1002/grl.50502, 2013.

Ibebuchi, C. C.: Circulation Patterns Linked to the Positive Sub-Tropical Indian Ocean Dipole, Adv. Atmos. Sci., 40, 110–128, 10.1007/s00376-022-2017-2, 2023.

Jain, P., Castellanos-Acuna, D., Coogan, S. C. P., Abatzoglou, J. T., and Flannigan, M. D.: Observed increases in extreme fire weather driven by atmospheric humidity and temperature, Nat. Clim. Chang., 12, 63–70, 10.1038/s41558-021-01224-1, 2022.

Jeong, Y.-C., Yeh, S.-W., Lim, Y.-K., Santoso, A., and Wang, G.: Indian Ocean warming as key driver of long-term positive trend of Arctic Oscillation, npj Climate and Atmospheric Science, 5, 56, 10.1038/s41612-022-00279-x, 2022.

Joiner, J. and Yoshida, Y.: Global MODIS and FLUXNET-derived Daily Gross Primary Production, V2 (Version 2) [dataset], 2021.

Kephe, P. N., Ayisi, K. K., and Petja, B. M.: Challenges and opportunities in crop simulation modelling under seasonal and projected climate change scenarios for crop production in South Africa, Agriculture & Food Security, 10, 10, 10.1186/s40066-020-00283-5, 2021.

Knutti, R., Furrer, R., Tebaldi, C., Cermak, J., and Meehl, G. A.: Challenges in Combining Projections from Multiple Climate Models, Journal of Climate, 23, 2739–2758, https://doi.org/10.1175/2009JCLI3361.1, 2010.

Kruger, A. C. and Nxumalo, M. P.: Historical rainfall trends in South Africa: 1921–2015, Water SA, 43, 285–297, 10.4314/wsa.v43i2.12, 2017.

Kusangaya, S., Warburton, M. L., Archer van Garderen, E., and Jewitt, G. P. W.: Impacts of climate change on water resources in southern Africa: A review, Physics and Chemistry of the Earth, Parts A/B/C, 67-69, 47–54, https://doi.org/10.1016/j.pce.2013.09.014, 2014.

Lawrence, B. N., Bennett, V., Churchill, J., Juckes, M., Kershaw, P., Oliver, P., Pritchard, M., and Stephens, A.: The JASMIN super-data-cluster, arXiv preprint arXiv:1204.3553, 2012.

Lewinschal, A., Ekman, A. M. L., and Körnich, H.: The role of precipitation in aerosol-induced changes in northern hemisphere wintertime stationary waves, Clim Dyn, 41, 647–661, 10.1007/s00382-012-1622-7, 2013.

Li, C., McLinden, C., Fioletov, V., Krotkov, N., Carn, S., Joiner, J., Streets, D., He, H., Ren, X., Li, Z., and Dickerson, R. R.: India Is Overtaking China as the World's Largest Emitter of Anthropogenic Sulfur Dioxide, Scientific Reports, 7, 14304, 10.1038/s41598-017-14639-8, 2017.

Li, G., Xie, S.-P., and Du, Y.: Monsoon-Induced Biases of Climate Models over the Tropical Indian Ocean, Journal of Climate, 28, 3058–3072, https://doi.org/10.1175/JCLI-D-14-00740.1, 2015.

Li, Z., Lau, W. K. M., Ramanathan, V., Wu, G., Ding, Y., Manoj, M. G., Liu, J., Qian, Y., Li, J., Zhou, T., Fan, J., Rosenfeld, D., Ming, Y., Wang, Y., Huang, J., Wang, B., Xu, X., Lee, S. S., Cribb, M., Zhang, F., Yang, X., Zhao, C., Takemura, T., Wang, K., Xia, X., Yin, Y., Zhang, H., Guo, J., Zhai, P. M., Sugimoto, N., Babu, S. S., and Brasseur, G. P.: Aerosol and monsoon climate interactions over Asia, Reviews of Geophysics, 54, 866–929, https://doi.org/10.1002/2015RG000500, 2016.

Lim Kam Sian, K. T., Wang, J., Ayugi, B. O., Nooni, I. K., and Ongoma, V.: Multi-Decadal Variability and Future Changes in Precipitation over Southern Africa, 10.3390/atmos12060742, 2021.

Lin, W., Yuan, H., Dong, W., Zhang, S., Liu, S., Wei, N., Lu, X., Wei, Z., Hu, Y., and Dai, Y.: Reprocessed MODIS Version 6.1 Leaf Area Index Dataset and Its Evaluation for Land Surface and Climate Modeling, 10.3390/rs15071780, 2023.

Liu, L., Shawki, D., Voulgarakis, A., Kasoar, M., Samset, B. H., Myhre, G., Forster, P. M., Hodnebrog, Ø.,

https://doi.org/10.5194/egusphere-2026-2198
Preprint. Discussion started: 20 May 2026

Sillmann, J., Aalbergsjø, S. G., Boucher, O., Faluvegi, G., Iversen, T., Kirkevåg, A., Lamarque, J. F., Olivié, D., Richardson, T., Shindell, D., and Takemura, T.: A PDRMIP Multimodel Study on the Impacts of Regional Aerosol Forcings on Global and Regional Precipitation, Journal of Climate, 31, 4429–4447, https://doi.org/10.1175/JCLI-D-17-0439.1, 2018.

Liu, Z., Bollasina, M. A., and Wilcox, L. J.: Impact of Asian aerosols on the summer monsoon strongly modulated by regional precipitation biases, Atmos. Chem. Phys., 24, 7227–7252, 10.5194/acp-24-7227-2024, 2024.

MacKellar, N., New, M., and Jack, C.: Observed and modelled trends in rainfall and temperature for South Africa: 1960–2010, South African Journal of Science, 110, 13, 10.1590/sajs.2014/20130353, 2014.

Maidment, R. I., Grimes, D., Black, E., Tarnavsky, E., Young, M., Greatrex, H., Allan, R. P., Stein, T., Nkonde, E., Senkunda, S., and Alcántara, E. M. U.: A new, long-term daily satellite-based rainfall dataset for operational monitoring in Africa, Scientific Data, 4, 170063, 10.1038/sdata.2017.63, 2017.

Marumbwa, F. M., Cho, M. A., and Chirwa, P. W.: Analysis of spatio-temporal rainfall trends across southern African biomes between 1981 and 2016, Physics and Chemistry of the Earth, Parts A/B/C, 114, 102808, https://doi.org/10.1016/j.pce.2019.10.004, 2019.

McDuffie, E. E., Smith, S. J., O'Rourke, P., Tibrewal, K., Venkataraman, C., Marais, E. A., Zheng, B., Crippa, M., Brauer, M., and Martin, R. V.: A global anthropogenic emission inventory of atmospheric pollutants from sector- and fuel-specific sources (1970–2017): an application of the Community Emissions Data System (CEDS), Earth System Science Data, 12, 3413–3442, 10.5194/essd-12-3413-2020, 2020.

Munday, C., Washington, R., Engelstaedter, S., Zilli, M., Harbord, S., Knight, C., Attwood, K., and Hart, N.: Southern African Climate Change: Processes, Models, and Projections, WIREs Climate Change, 16, e70025, https://doi.org/10.1002/wcc.70025, 2025.

Myhre, G., Forster, P. M., Samset, B. H., Hodnebrog, Ø., Sillmann, J., Aalbergsjø, S. G., Andrews, T., Boucher, O., Faluvegi, G., Fläschner, D., Iversen, T., Kasoar, M., Kharin, V., Kirkevåg, A., Lamarque, J. F., Olivié, D., Richardson, T. B., Shindell, D., Shine, K. P., Stjern, C. W., Takemura, T., Voulgarakis, A., and Zwiers, F.: PDRMIP: A Precipitation Driver and Response Model Intercomparison Project—Protocol and Preliminary Results, Bulletin of the American Meteorological Society, 98, 1185–1198, https://doi.org/10.1175/BAMS-D-16-0019.1, 2017.

Niles, M. T., Lubell, M., and Brown, M.: How limiting factors drive agricultural adaptation to climate change, Agriculture, Ecosystems & Environment, 200, 178–185, 10.1016/j.agee.2014.11.010, 2015.

Palmer, P. I., Wainwright, C. M., Dong, B., Maidment, R. I., Wheeler, K. G., Gedney, N., Hickman, J. E., Madani, N., Folwell, S. S., Abdo, G., Allan, R. P., Black, E. C. L., Feng, L., Gudoshava, M., Haines, K., Huntingford, C., Kilavi, M., Lunt, M. F., Shaaban, A., and Turner, A. G.: Drivers and impacts of Eastern African rainfall variability, Nature Reviews Earth & Environment, 4, 254–270, 10.1038/s43017-023-00397-x, 2023.

Quagraine, K. A., Hewitson, B., Jack, C., Pinto, I., and Lennard, C.: A Methodological Approach to Assess the Co-Behavior of Climate Processes over Southern Africa, Journal of Climate, 32, 2483–2495, 10.1175/JCLI-D-18-0689.1, 2019.

Randriatsara, H. H.-R. H., Hu, Z., Ayugi, B., Makula, E. K., Vuguziga, F., and Nkunzimana, A.: Interannual characteristics of rainfall over Madagascar and its relationship with the Indian Ocean sea surface temperature variation, Theor Appl Climatol, 148, 349–362, 10.1007/s00704-022-03950-8, 2022.

Ribeiro, A. F. S., Brando, P. M., Santos, L., Rattis, L., Hirschi, M., Hauser, M., Seneviratne, S. I., and Zscheischler, J.: A compound event-oriented framework to tropical fire risk assessment in a changing climate, Environ. Res. Lett., 17, 065015, 10.1088/1748-9326/ac7342, 2022.

Rustemeier, E., Finger, P., Schirmeister, Z., and Ziese, M.: GPCC Precipitation Analysis Monthly Version 2025

https://doi.org/10.5194/egusphere-2026-2198
Preprint. Discussion started: 20 May 2026

at 1.0°: Monthly Land-Surface Precipitation Analysis for every Month from Rain-Gauges built on GTS-based and Historical Data [dataset], 10.5676/DWD_GPCC/MONTHLY_V2025_100, 2025.

Saha, A. and Ghosh, S.: Can the weakening of Indian Monsoon be attributed to anthropogenic aerosols?, Environmental Research Communications, 1, 061006, 10.1088/2515-7620/ab2c65, 2019.

Samset, B. H., Lund, M. T., Bollasina, M., Myhre, G., and Wilcox, L.: Emerging Asian aerosol patterns, Nature Geosci, 12, 582–584, 10.1038/s41561-019-0424-5, 2019.

Samset, B. H., Wilcox, L. J., Allen, R. J., Stjern, C. W., Lund, M. T., Ahmadi, S., Ekman, A., Elling, M. T., Fraser-Leach, L., Griffiths, P., Keeble, J., Koshiro, T., Kushner, P., Lewinschal, A., Makkonen, R., Merikanto, J., Nabat, P., Narazenko, L., O'Donnell, D., Oshima, N., Rumbold, S. T., Takemura, T., Tsigaridis, K., and Westervelt, D. M.: East Asian aerosol cleanup has likely contributed to the recent acceleration in global warming, Communications Earth & Environment, 6, 543, 10.1038/s43247-025-02527-3, 2025.

Shikwambana, L., Mhangara, P., and Mbatha, N.: Trend analysis and first time observations of sulphur dioxide and nitrogen dioxide in South Africa using TROPOMI/Sentinel-5 P data, International Journal of Applied Earth Observation and Geoinformation, 91, 102130, https://doi.org/10.1016/j.jag.2020.102130, 2020.

Shindell, D. T., Voulgarakis, A., Faluvegi, G., and Milly, G.: Precipitation response to regional radiative forcing, Atmospheric Chemistry and Physics, 12, 6969–6982, 10.5194/acp-12-6969-2012, 2012.

Shonk, J. K. P., Turner, A. G., Chevuturi, A., Wilcox, L. J., Dittus, A. J., and Hawkins, E.: Uncertainty in aerosol radiative forcing impacts the simulated global monsoon in the 20th century, Atmospheric Chemistry and Physics, 20, 14903–14915, 10.5194/acp-20-14903-2020, 2020.

Sintayehu, D. W.: Impact of climate change on biodiversity and associated key ecosystem services in Africa: a systematic review, Ecosystem Health and Sustainability, 4, 225–239, 10.1080/20964129.2018.1530054, 2018.

Smith, C. J., Kramer, R. J., Myhre, G., Alterskjær, K., Collins, W., Sima, A., Boucher, O., Dufresne, J. L., Nabat, P., Michou, M., Yukimoto, S., Cole, J., Paynter, D., Shiogama, H., O'Connor, F. M., Robertson, E., Wiltshire, A., Andrews, T., Hannay, C., Miller, R., Nazarenko, L., Kirkevåg, A., Olivié, D., Fiedler, S., Lewinschal, A., Mackallah, C., Dix, M., Pincus, R., and Forster, P. M.: Effective radiative forcing and adjustments in CMIP6 models, Atmos. Chem. Phys., 20, 9591–9618, 10.5194/acp-20-9591-2020, 2020.

Sreekala, P. P., Babu, C. A., and Rao, S. V. B.: On the simulation of northeast monsoon rainfall over southern peninsular India in CMIP5 and CMIP6 models, Theor Appl Climatol, 150, 969–986, 10.1007/s00704-022-04194-2, 2022.

Stier, P., van den Heever, S. C., Christensen, M. W., Gryspeerdt, E., Dagan, G., Saleeby, S. M., Bollasina, M., Donner, L., Emanuel, K., Ekman, A. M. L., Feingold, G., Field, P., Forster, P., Haywood, J., Kahn, R., Koren, I., Kummerow, C., L'Ecuyer, T., Lohmann, U., Ming, Y., Myhre, G., Quaas, J., Rosenfeld, D., Samset, B., Seifert, A., Stephens, G., and Tao, W.-K.: Multifaceted aerosol effects on precipitation, Nature Geosci, 17, 719–732, 10.1038/s41561-024-01482-6, 2024.

Sun, W., Bollasina, M. A., Colfescu, I., Wu, G., and Liu, Y.: European sulphate aerosols were a key driver of the early twentieth-century intensification of the Asian summer monsoon, Atmos. Chem. Phys., 26, 2027–2039, 10.5194/acp-26-2027-2026, 2026.

Thoithi, W., Blamey, R. C., and Reason, C. J. C.: Dry Spells, Wet Days, and Their Trends Across Southern Africa During the Summer Rainy Season, Geophysical Research Letters, 48, e2020GL091041, https://doi.org/10.1029/2020GL091041, 2021.

Twomey, S.: The Influence of Pollution on the Shortwave Albedo of Clouds, Journal of the Atmospheric Sciences, 34, 1149–1152, 10.1175/1520-0469(1977)034<1149:TIOPOT>2.0.CO;2, 1977.

https://doi.org/10.5194/egusphere-2026-2198
Preprint. Discussion started: 20 May 2026

738 Undorf, S., Polson, D., Bollasina, M. A., Ming, Y., Schurer, A., and Hegerl, G. C.: Detectable Impact of Local
739 and Remote Anthropogenic Aerosols on the 20th Century Changes of West African and South Asian
740 Monsoon Precipitation, Journal of Geophysical Research: Atmospheres, 123, 4871–4889,
741 10.1029/2017JD027711, 2018.
742 Voigt, A., Pincus, R., Stevens, B., Bony, S., Boucher, O., Bellouin, N., Lewinschal, A., Medeiros, B., Wang, Z.,
743 and Zhang, H.: Fast and slow shifts of the zonal-mean intertropical convergence zone in response to an
744 idealized anthropogenic aerosol, Journal of Advances in Modeling Earth Systems, 9, 870–892,
745 10.1002/2016MS000902, 2017.
746 Wang, Z., Xue, L., Liu, J., Ding, K., Lou, S., Ding, A., Wang, J., and Huang, X.: Roles of Atmospheric Aerosols
747 in Extreme Meteorological Events: a Systematic Review, Current Pollution Reports, 8, 177–188,
748 10.1007/s40726-022-00216-9, 2022.
749 Wilcox, L. J., Dunstone, N., Lewinschal, A., Bollasina, M., Ekman, A. M. L., and Highwood, E. J.: Mechanisms
750 for a remote response to Asian anthropogenic aerosol in boreal winter, Atmospheric Chemistry and Physics,
751 19, 9081–9095, 10.5194/acp-19-9081-2019, 2019.
752 Wimberly, M. C., Wanyama, D., Doughty, R., Peiro, H., and Crowell, S.: Increasing Fire Activity in African
753 Tropical Forests Is Associated With Deforestation and Climate Change, Geophysical Research Letters, 51,
754 e2023GL106240, https://doi.org/10.1029/2023GL106240, 2024.
755 Xie, P. and Arkin, P. A.: Global Precipitation: A 17-Year Monthly Analysis Based on Gauge Observations,
756 Satellite Estimates, and Numerical Model Outputs, Bulletin of the American Meteorological Society, 78,
757 2539–2558, https://doi.org/10.1175/1520-0477(1997)078<2539:GPAYMA>2.0.CO;2, 1997.
758 Yoo, S.-H., Yang, S., and Ho, C.-H.: Variability of the Indian Ocean sea surface temperature and its impacts on
759 Asian-Australian monsoon climate, Journal of Geophysical Research: Atmospheres, 111,
760 https://doi.org/10.1029/2005JD006001, 2006.
761 Zhang, S., Stier, P., Dagan, G., and Wang, M.: Anthropogenic Aerosols Modulated 20th-Century Sahel Rainfall
762 Variability Via Their Impacts on North Atlantic Sea Surface Temperature, Geophysical Research Letters,
763 49, e2021GL095629, 10.1029/2021GL095629, 2022.
764 Zheng, Y., Zhang, Q., Tong, D., Davis, S. J., and Caldeira, K.: Climate effects of China's efforts to improve its
765 air quality, Environ. Res. Lett., 15, 104052, 10.1088/1748-9326/ab9e21, 2020.
766 Zhou, S., Williams, A. P., Lintner, B. R., Berg, A. M., Zhang, Y., Keenan, T. F., Cook, B. I., Hagemann, S.,
767 Seneviratne, S. I., and Gentine, P.: Soil moisture–atmosphere feedbacks mitigate declining water
768 availability in drylands, Nat. Clim. Chang., 11, 38–44, 10.1038/s41558-020-00945-z, 2021.

769